Using radar altimetry to update a large-scale hydrological model of the Brahmaputra river basin

Flemming Finsen, Christian Milzow, Richard Smith, Philippa Berry and Peter Bauer-Gottwein

ABSTRACT

Measurements of river and lake water levels from space-borne radar altimeters (past missions include ERS, Envisat, Jason, Topex) are useful for calibration and validation of large-scale hydrological models in poorly gauged river basins. Altimetry data availability over the downstream reaches of the Brahmaputra is excellent (17 high-quality virtual stations from ERS-2, 6 from Topex and 10 from Envisat are available for the Brahmaputra). In this study, altimetry data are used to update a large-scale Budyko-type hydrological model of the Brahmaputra river basin in real time. Altimetry measurements are converted to discharge using rating curves of simulated discharge versus observed altimetry. This approach makes it possible to use altimetry data from river cross sections where both in-situ rating curves and accurate river cross section geometry are not available. Model updating based on radar altimetry improved model performance considerably. The Nash–Sutcliffe model efficiency increased from 0.77 to 0.83. Real-time river basin modelling using radar altimetry has the potential to improve the predictive capability of large-scale hydrological models elsewhere on the planet.

Key words | Brahmaputra, large-scale hydrological model, radar altimetry, real-time updating

Flemming Finsen
Christian Milzow
Peter Bauer-Gottwein (corresponding author)
Department of Environmental Engineering,
Technical University of Denmark,
2800 Kgs. Lyngby,
Denmark
E-mail: *pbau@env.dtu.dk*

Richard Smith
Philippa Berry
Earth and Planetary Remote Sensing Laboratory,
De Montfort University,
The Gateway,
Leicester,
LE1 9BH,
UK

INTRODUCTION

Large-scale hydrological models have been developed for the majority of the planet's major river basins. The reported modelling studies have been motivated by two main purposes: (1) to understand large-scale hydrological dynamics and (2) to support water resources management. Continental to global-scale modelling work for purpose 1 has been driven by the need to represent accurately the land phase of the hydrological cycle in global climate models. Most recent climate models include sophisticated land surface schemes (e.g. GLDAS (Rodell *et al.* 2004) and CLM (Oleson *et al.* 2008)), and some of them were coupled to river routing components to simulate river discharge at the global scale (e.g. Nohara *et al.* 2006; Qian *et al.* 2006). Continental to global-scale modelling work for purpose 2 has been motivated by the need to produce global water availability and water stress information to promote political and public awareness of global water problems (e.g. WaterGAP; Alcamo *et al.* 2003).

At the river basin scale, the dominant motivation for hydrological modelling studies is decision support to water resources managers. In the context of the integrated water resources management paradigm, it has been widely recognized that water resources management must operate at the scale of the river basin, even if the basin extends over various administrative units or nations. In highly developed and well-monitored water resources systems, management models typically do not include a rainfall–runoff modelling component. Instead, the models are forced with observed inflows or with stochastic inflow time series, which are generated based on observed runoff statistics. Good examples of such models are the regional information system on water and land resources for the Aral Sea basin (Dukhovny *et al.* 2004) and the CALVIN model used to support water resources management in California (Draper *et al.* 2003). Many of the world's major river basins are, however, poorly

doi: 10.2166/nh.2013.191

monitored. Decision support systems in such basins should include a rainfall–runoff modelling component. With the advent of global-scale precipitation products based on remote sensing and reanalysis technology (see Stisen & Sandholt (2010) for a recent review) rainfall–runoff modelling in poorly monitored basins has become feasible. Rainfall–runoff models typically use lumped conceptual representations of the hydrological cycle. Some approaches are purely heuristic (e.g. the Budyko framework; Zhang *et al.* 2008), while others use a more physically based representation (e.g. NAM; Refsgaard & Knudsen 1996). Due to the large inherent uncertainties in the precipitation forcing, particularly in mountainous regions, and the significant structural errors in the rainfall–runoff models, river discharge predictions from such models are typically not good enough for water resources management purposes. While the models pick up seasonal variations and overall hydrological dynamics, they fail to reproduce accurately extreme events such as floods and droughts, which are most relevant in the context of water resources management.

These shortcomings provide the motivation to investigate and explore the potential of innovative data sources based on remote sensing to inform regional-scale hydrological models in a real-time data assimilation framework. Assimilation of remote sensing data has become standard practice in the atmospheric and ocean modelling communities. For instance, in the MyOcean component of the European Commission's Global Monitoring for Environment and Security programme (GMES), real-time ocean monitoring and forecasting are provided to a user community, based on in-situ data, remote sensing data and ocean models. Real-time data assimilation techniques are also well established in the river modelling community (e.g. Madsen & Skotner 2005; Vrugt *et al.* 2005). However, in most applications, in-situ water levels or discharges from automatic gauging stations are assimilated. Published studies assimilating remotely sensed water levels fall into two categories: Assimilation studies using water level maps derived from synthetic aperture radar (SAR) images (e.g. Hostache *et al.* 2009; Mason *et al.* 2009; Schumann *et al.* 2011) and assimilation studies using synthetic swath altimetry observations (e.g. Andreadis *et al.* 2007; Durand *et al.* 2008; Biancamaria *et al.* 2011), motivated mainly by the upcoming Surface Water and Ocean Topography (SWOT) mission. Recently, inland water level products based on space-borne radar altimeters (ERS, Envisat, Jason, Topex) have been developed. Such products are available from three websites: ESA River and Lake (Berry *et al.* 2005), CNES Hydroweb (Cretaux *et al.* 2011) and CropExplorer USA Global Reservoir and Lake Elevation Database (Coe & Birkett 2004). Radar altimeter measurements can be processed in near real time and can complement in-situ river level data in poorly gauged basins. Depending on the size of the river and the orbit configuration, the accuracy of water levels measured with radar altimeters ranges from better than 10 cm to more than one metre. Assimilation of such data types into river models is similar to the assimilation of in-situ water levels. Significant differences exist in terms of the spatio-temporal resolution of the data. While in-situ data are typically available from a limited number of observation points at high temporal resolution, radar altimetry data are available from many virtual stations at low temporal resolution (e.g. 35 days for Envisat). The term 'virtual station' refers to an intersection point between the ground track of a satellite carrying the nadir-looking altimeter and a surface water body. However, the low temporal resolution is partly balanced by constant temporal offsets between the different virtual stations, which are due to the satellite orbit configuration. Several studies have evaluated the performance of radar altimetry for specific river systems (e.g. Birkett *et al.* 2002; Maheu *et al.* 2003; Birkinshaw *et al.* 2010). While most of these studies focused on large rivers (e.g. Amazon, Mekong River), Milzow *et al.* (2011) obtained good results for rivers as narrow as 150 m in the Okavango river basin. The study by Pereira-Cardenal *et al.* (2011) is an example of successful assimilation of radar altimetry measurements over reservoirs into a basin-scale hydrological model. The present study is one of the first to combine nadir radar altimetry data and a hydrological model into an operational forecasting scheme for large river basins. The study uses a simple heuristic assimilation procedure that does not provide or evaluate forecast uncertainty. However, the results show that a forecast using both the model and the altimetry data outperforms forecasts produced by the model or the altimeter alone.

The Brahmaputra river basin

The Brahmaputra River originates north of the main chain of the Himalayan mountain range and flows east through Tibet for approximately 1,500 km. The Tibetan portion of

the river is known as Yarlung Tsangpo. At the Chinese/Indian border, in the Indian federal state of Arunachal Pradesh, the river changes its course to westbound and crosses the border between India and Bangladesh before merging with the Ganges into the Meghna and flowing into the Bay of Bengal (Figure 1). In Bangladesh, the river is known as the Jamuna River.

A number of previous modelling efforts have been reported for the Brahmaputra and Ganges river systems. Nishat & Rahman (2009) set up a water resources management model in MIKE BASIN, over the Ganges, Brahmaputra and Meghna (GBM) river basins. They demonstrate that it is possible to calibrate MIKE BASIN to a satisfactory level and predict flow in the Ganges and Brahmaputra rivers at the entry points of Bangladesh at relevant scales for water resources management. Rao *et al.* (2009) used the Hydrologic Modelling System (HEC-HMS 3.0.1) to simulate water flow in the Brahmaputra basin together with satellite-based rainfall products and the Shuttle Radar Topography Mission Digital Elevation Model (SRTM DEM). Akhtar *et al.* (2009) have carried out a comparative analysis of multiple artificial neural network (ANN) models with different hydrological pre-processing for the Ganges river basin. The ANN showed its ability to forecast discharges 3 days ahead with an acceptable accuracy. Within this forecast horizon, the influence of the pre-processed rainfall is marginal, because of dominant influence of strongly auto-correlated discharge inputs. For forecast horizons of 7 to 10 days, the influence of the pre-processed rainfall is noticeable, although the overall model performance deteriorates. Mondal & Wasimi (2006) use periodic autoregressive (PAR) models to capture the seasonal

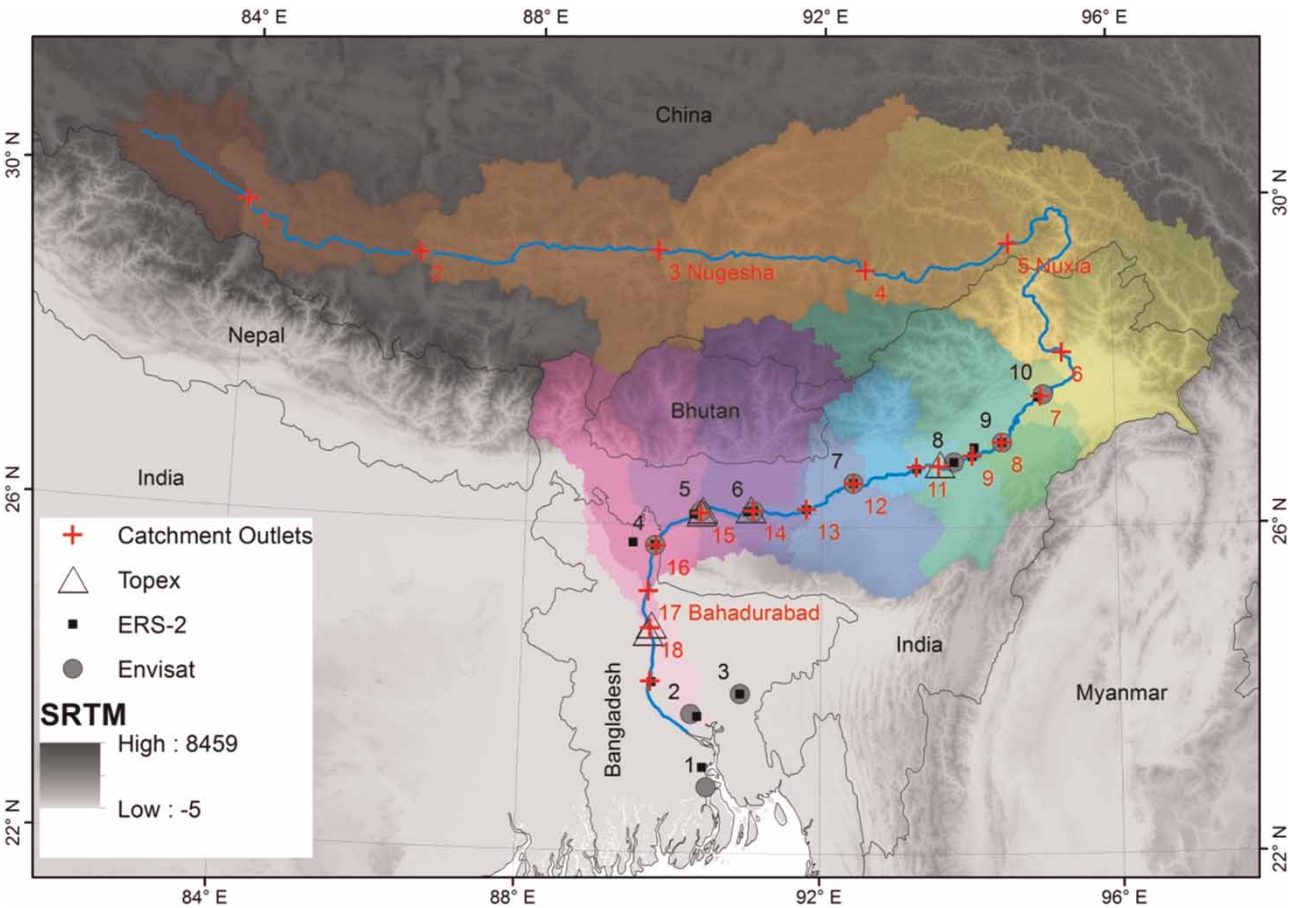

Figure 1 | Base map of the Brahmaputra river basin. Subcatchment outlets of the hydrological model are shown as crosses. Envisat altimetry targets are shown as filled circles. Numeric labels on the left side of the river refer to catchment outlets, numeric labels on the right side of the river refer to Envisat altimetry targets. Topex and ERS-2 targets are not labelled. The background shading indicates SRTM elevation in mamsl.

variability of the Ganges River flow. The model performs reasonably well, preserving both its short- and long-term important historical statistics. For the Bangladeshi part of the Brahmaputra River, a detailed river model exists, which is implemented in the DHI software Mike-11 (Jakobsen *et al.* 2005). However, this model is classified for national security reasons and is not accessible to the research community.

The main motivation for hydrological modelling in the region is to improve the prediction of flood waves in the rivers, which are a significant threat to life, property and infrastructure in the affected regions.

MATERIALS AND METHODS

Hydrological modelling approach

The hydrological model consists of a snow storage compartment, a rainfall–runoff compartment and a river flow compartment. Figure 2 presents an overall modelling flow chart. A lumped-parameter semi-distributed approach is used because of limited availability of in-situ data and for reasons of computational efficiency. In total, 19 sub-basins were defined. The outlet points of the sub-basins correspond to the available Envisat radar altimetry targets and to available in-situ monitoring stations. The Brahmaputra basin was divided into an upstream part (sub-basins 1–6) and a downstream part (sub-basins 7–19). This division was motivated by calibration data availability and geography: The upstream part is located north of the main chain of the Himalayan range, while the downstream part is located south of the main chain and is dominated by a monsoon climate. Significant orographic effects are expected for the precipitation in the downstream portion.

Snow melt modelling

Snow accumulation and melt processes were implemented using a simple temperature index method (Hock 2003). Precipitation falls as snow if the air temperature is below the threshold of 0 °C. Each sub-catchment is divided into 10 elevation zones and the air temperature is computed for each elevation zone using a temperature lapse rate of 5 degrees per kilometre. The precipitation is corrected for elevation using a constant precipitation lapse rate of

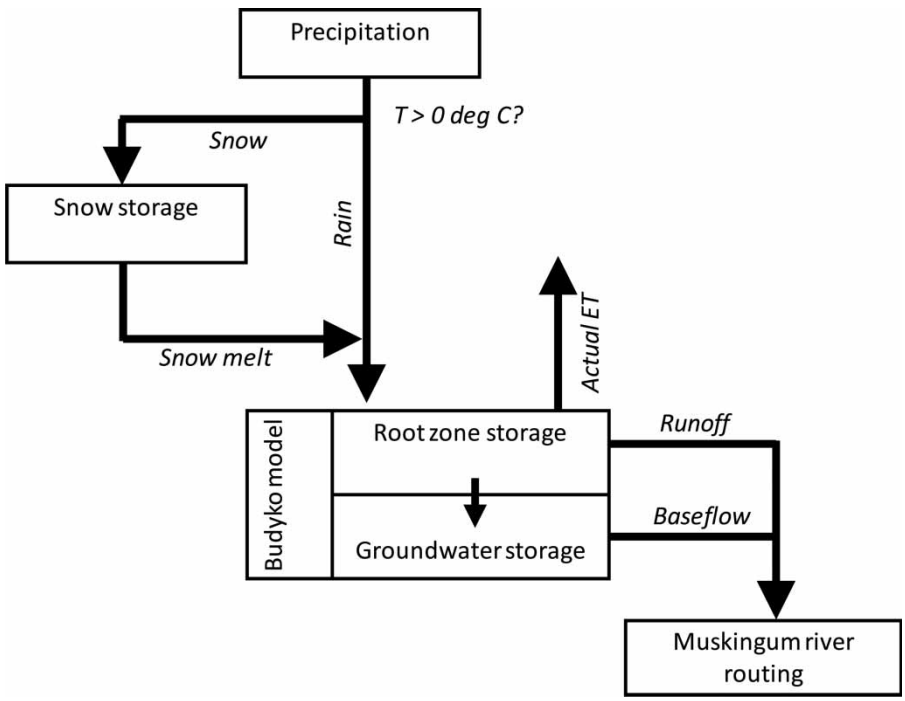

Figure 2 | Flow chart of the Brahmaputra river basin model.

100 mm/yr per kilometre elevation change. Precipitation correction terms are constant in time and are added to all daily precipitation records showing significant amounts of precipitation. The precipitation correction procedure is equivalent to the correction procedure used in the well-recognized SWAT (Soil and Water Assessment Tool) hydrological simulation package (Arnold *et al.* 1998). Snowmelt occurs whenever the air temperature in the respective elevation zone is above 0 °C. Snow melt is computed using a constant degree-day factor of 1.5 mm per degree per day.

Rainfall–runoff modelling

The sum of direct precipitation and snowmelt enters the rainfall–runoff model. For each sub-basin, the model uses a heuristic, lumped-parameter approach based on the Budyko framework (Zhang *et al.* 2008). The model operates with two storage compartments: a root zone storage and a groundwater storage. Budyko's limits concept (Budyko 1958) is applied (1) to partition precipitation into catchment retention and direct runoff, (2) to compute groundwater recharge from catchment retention and soil storage carried over from the last time step and (3) to partition soil water availability into actual evapotranspiration and soil storage carried over to the next time step. The rainfall–runoff model requires four input parameters per sub-catchment. All four parameters of the rainfall–runoff model were calibrated. For details on the rainfall–runoff model, please consult the Zhang *et al.* (2008) reference.

River network modelling

Only the main Brahmaputra River channel was simulated in the model, because no calibration or validation datasets were available from the tributaries and the radar altimetry targets of interest are all located on the main channel. The discharge was routed from one catchment outlet node to the next using Muskingum–Cunge river routing (e.g. Chow *et al.* 1988). Routing time constants of individual river segments are based on segment lengths and on average river flow velocity. Average river flow velocities in the upstream and downstream portions of the basin are calibrated. The Muskingum weighting factor was also calibrated for both the upstream and the downstream portions of the basin.

Water use

Water use for irrigation, domestic and industrial purposes is not simulated in the model. This can be justified because the main purpose of this study is improved prediction of peak flows using radar altimetry. Peak flows at the Bahadurabad station are on the order of 50,000 $m^3 s^{-1}$, about 10 times higher than average low flows. While water use likely has a significant impact on low flows, peak flows are not expected to be significantly affected. During the peak flow period, model errors due to uncertainties in the precipitation product (see the discussion of the precipitation input below) and structural errors due to the parameterization of the rainfall–runoff processes are most likely much larger than abstractions for water use.

Model input and calibration/validation datasets

Digital Elevation Model and catchment delineation

A DEM was obtained from the NASA SRTM. The SRTM DEM has a spatial resolution of 3 arcseconds and was downloaded as a 5×5 degree mosaic (http://srtm.csi.cgiar.org/). The data were resampled to a resolution of 30 arcseconds in order to keep the processing time for the DEM hydro-processing routine at a reasonable level. Subsequently, the drainage network and the sub-basins were derived from the DEM using a MATLAB DEM hydro-processing routine (TopoToolbox; Schwanghart & Kuhn 2010).

Precipitation

The Tropical Rainfall Measuring Mission (TRMM) Multi-satellite Precipitation Analysis (TMPA) was used as precipitation forcing dataset. This dataset combines the TRMM precipitation radar, the TRMM microwave imager, the TRMM visible infrared scanner and infrared sensors from various other missions (Huffman *et al.* 2007). Gridded precipitation between 50 degrees south and 50 degrees north is provided. The TMPA offers two products: the 3B42 product and the 3B42RT real-time product, both of which have a spatial resolution of 0.25 degrees and a temporal resolution of 3 hours. The product estimates total precipitation,

i.e. the sum of rain and snow. Because the hydrological model was designed for real-time applications, the 3B42RT product was chosen as the primary precipitation forcing. However, 3B42RT was only available from October 2008 onwards. In order to extend the model calibration period, the 3B42 product was used to force the model in the period from January 2000 to September 2008. Spatio-temporal rainfall patterns of the two products are similar because they are based on the same set of remote sensing observations. Any bias between the two precipitation products had to be removed because simulated water balances would otherwise be different for the calibration and forecasting periods. To compute the bias, total precipitation amounts between October 2008 and June 2011 were compared between the 3B42 and 3B42RT products for the Brahmaputra river basin. On average 3B42RT precipitation was 25% higher than 3B42 precipitation. Consequently pre-October 2008 3B42 data were scaled by a factor of 1.25 and were used to force the hydrological model in the period January 2000 to September 2008. After October 2008, the 3B42RT product was used as the precipitation input in the hydrological model.

Using this precipitation dataset, average runoff coefficients at Nuxia and Bahadurabad were calculated. The total long-term average precipitation upstream of Nuxia is 4,483 $m^3 s^{-1}$, while the long-term average observed discharge at Nuxia is 2,000 $m^3 s^{-1}$ (Montgomery *et al.* 2004). The resulting runoff coefficient is 0.45. Total long-term average precipitation between Nuxia and Bahadurabad is 16,616 $m^3 s^{-1}$. The long-term average flow at Bahadurabad is 20,408 $m^3 s^{-1}$, which results in a runoff coefficient of the downstream portion equal to 1.11. This clearly is an unreasonable runoff coefficient and the precipitation in the downstream portion of the basin was multiplied by a factor of 1.7 to achieve similar runoff coefficients as in the upstream part of the river basin. The bias of the precipitation product in the downstream portions of the basin might be due to strong topographic gradients and orographic lifting of air masses during the monsoon, which may not be captured sufficiently accurately by the TMPA products in the Brahmaputra river basin. This ad-hoc bias correction procedure is debatable and may be changed if more hydroclimatological data become available. It is considered acceptable here because this paper focuses on operational discharge forecasting and not on understanding regional hydrological processes.

Temperature

Real-time temperature data are obtained from the European Centre for Medium-Range Weather Forecast (ECMWF) Operational Surface Analysis Data Set. The dataset includes 6 hourly data for 2 m temperature with a 0.5 degree spatial resolution (approximately 54 km at the equator) until 2006 and a 0.25 degree (27.7 km) resolution from 2006 onwards. The data were provided via ftp in real time by the Danish Metrological Institute. Maximum and minimum daily temperatures are used to calculate reference ET using Hargreaves' equation (Hargreaves & Samani 1982). Daily minimum and maximum temperatures were assumed to be equal to the maximum and minimum temperatures in the 6-hourly temperature record for each day.

In-situ river gauge data

In-situ river discharge data are extremely hard to obtain for the Brahmaputra. Only a small amount of data is in the public domain, because flooding data are classified information in Bangladesh. The Global Runoff Data Center (GRDC 2007) global database only includes very few historical datasets and no recent data. In-situ data are available for three stations: Nugesha, Nuxia and Bahadurabad (see Figure 1). Historical daily discharge data (1956–2000) for the Bahadurabad station were downloaded from http://cfab.eas.gatech.edu/Raingage/Q_Bahadurabad.txt. For the recent flooding seasons, daily observed discharge data are published on http://cfab.eas.gatech.edu/shortterm/ensemble.html. During the baseflow period (December to April) variability in the observed historical discharge from 1956 to 2000 is small. Thus, for recent years, baseflow was estimated as the historical average flow in the Brahmaputra River for the corresponding day of the year in order to provide a baseflow time series for calibration. Data for two stations in Tibet (Nuxia and Nugesha) are available for the high flow periods of 2005, 2006 and 2007. The data have been downloaded from http://southasianfloods.icimod.org/saf/reports/. In-situ water levels for the station Bahadurabad for the time period 1995 to 2003 were provided by the Institute of Water Modelling in Dhaka, Bangladesh.

Radar altimetry data

Radar altimetry time series were extracted from ERS-2, Topex and Envisat data over the Brahmaputra based on an updated map of potential open water surfaces derived from automatic river network delineation from the SRTM elevation map. Retrieval was carried out using the waveform analysis and retracking algorithms developed in the ESA-funded River and Lake project. These enable identification of radar echoes from open water surfaces, and successfully convert these to yield inland water heights. Retrieval algorithms are described in Berry *et al.* 2005 and global radar altimetry data availability is documented on the River and Lake webpage at earth.esa.int/riverandlake. In order to check quality and consistency of the radar altimetry dataset, the kinematic wave travel times (delay times) between the various upstream altimetry targets and the in-situ gauging station Bahadurabad on the Brahmaputra were determined using the following procedure: the correlation between the water levels from the virtual station and the in-situ station is:

$$\mathrm{CC} = \frac{\frac{1}{n}\sum_{i=1}^{n}\left[y_A(t_i + t_{\mathrm{delay}}) - \bar{y}_A\right]\left[y_S(t_i) - \bar{y}_S\right]}{\sqrt{\frac{1}{n}\sum_{i=1}^{n}\left[y_A(t_i) - \bar{y}_A\right]^2}\cdot\sqrt{\frac{1}{n}\sum_{i=1}^{n}\left[y_S(t_i) - \bar{y}_S\right]^2}} \quad (1)$$

Here, CC (–) is the correlation coefficient between the two time series, which is a function of the applied delay time t_{delay}. The symbol y_A denotes the water level measured by the altimeter (m), y_S in m is the water level measured at the in-situ station. Overbars denote temporal averaging and n is the number of available altimetry measurements. The delay time is found by maximizing CC. A Nelder–Mead simplex search algorithm is used to perform the maximization (function fminsearch in MATLAB, Lagarias *et al.* 1998).

Confidence intervals on the determined t_{delay} are derived as follows:

$$t_{\mathrm{delay},l} = t_{\mathrm{delay}} \left| \mathrm{CC}(t_{\mathrm{delay}}) = \mathrm{CC}_{\max} + a \text{ and } t_{\mathrm{delay}} < t_{\mathrm{delay,max}} \right.$$
$$t_{\mathrm{delay},u} = t_{\mathrm{delay}} \left| \mathrm{CC}(t_{\mathrm{delay}}) = \mathrm{CC}_{\max} + a \text{ and } t_{\mathrm{delay}} > t_{\mathrm{delay,max}} \right. \quad (2)$$

Here, $t_{\mathrm{delay},l}$ is the lower bound of the confidence interval, $t_{\mathrm{delay},u}$ is the upper bound of the confidence interval, $\mathrm{CC}_{\max}$ is the maximum achieved correlation and $t_{\mathrm{delay,max}}$ is the delay for maximum correlation. The free parameter a was chosen as $a = -0.005$ in this study. The derived confidence intervals do not represent a given probability, but are useful to compare the reliability of the fitted values of t_{delay} at the different sites. The delay times could only be determined for the Topex and ERS-2 targets because the temporal overlap between the available in-situ water level records and the Envisat altimetry time series was too short.

Data assimilation

A simple heuristic assimilation strategy was developed. In the assimilation procedure, river discharge in the river segment corresponding to the assimilated altimetry target is updated. The internal states of the rainfall–runoff model (root zone storage, groundwater storage) are not updated. The assimilation procedure has three steps:

1. The calibrated model is executed and historical altimetry levels are plotted against simulated discharge on matching days for all altimetry targets. Subsequently, a power law of the form

$$Q = a(h - b)^c \quad (3)$$

is fitted to the plot, using a least-squares adjustment. In this formula, Q is the river discharge in $\mathrm{m^3\,s^{-1}}$, h is the altimetry water level in mamsl and a, b, c are fitting parameters. This rating curve is applied in the assimilation to convert altimetry water levels into altimetry-derived discharge. The underlying assumption is that the simulated river discharge is uncertain, but unbiased. The mean model error for the calibration period was +4% at Nuxia, –33% at Nugesha and –10.5% at Bahadurabad. Model bias is thus small, particularly for the downstream region, where all the radar altimetry targets are located.
2. The model is run in near real-time mode at daily time steps. Whenever an altimetry reading is available for any of the assimilated radar altimetry targets, the corresponding rating curve is used to convert the reading into a discharge estimate. The discharge in the corresponding river segment of the model is updated using the following equation:

$$Q_{\mathrm{ass}} = Q_{\mathrm{sim}} + G(Q_{\mathrm{alt}} - Q_{\mathrm{sim}}) \quad (4)$$

In this formula, Q_{ass} is the analysed discharge, Q_{sim} is the simulated discharge prior to assimilation, Q_{alt} is the discharge estimate based on altimetry and G is a gain factor ranging from 0 to 1.

3. The innovation $G(Q_{alt} - Q_{sim})$ is added to the simulated discharge at the river node representing the altimetry target. All updating terms are propagated to the next time step but are discounted in each time step using a constant discount factor δ, which was set to 0.975 per time step, using daily time steps. This value of the discount factor was found by trial-and-error adjustment, maximizing the Nash–Sutcliffe model efficiency.

RESULTS

Radar altimetry findings

Table 1 summarizes the characteristics of the virtual stations on the Brahmaputra River. 17 ERS-2 virtual stations, 6 Topex virtual stations and 10 Envisat virtual stations are available. The first column gives the altimetry target ID. The second column gives the relative overpass time, relative to the first ERS target (B-ERS-1). The third column gives the chainage of the altimetry target relative to the in-situ gauging station Bahadurabad. Negative numbers indicate a location upstream from the gauging station. The next two columns contain the geographic coordinates of the targets. The next column gives the approximate elevation of the target as read from the SRTM. The next three columns contain the fitted delay time and its lower and upper confidence interval bounds. The final column contains the maximum achieved correlation between the altimetry target and the discharge station. This correlation is achieved for a delay time as given in the table. Targets shaded in grey are considered outliers and were disregarded in the further analysis. They generally show a low degree of correlation with the in-situ gauging station and some of them are located on tributaries to the main river.

To illustrate the quality of the radar altimetry targets over the Brahmaputra, an example for target B-ERS-10 is shown in Figure 3. Although the target is located about 320 km upstream from the Bahadurabad station, correlation between the altimetry water level time series and the in-situ water level time series is very high. Figure 4 shows the delay times between the various altimetry targets and the Bahadurabad in-situ station as a function of river chainage. As expected, delay times increase with increasing distance from the in-situ station. Kinematic wave celerities can be extracted from the graph for three distinct sections of the Brahmaputra River. Given that the friction slope can be expressed using Manning's equation and assuming a uniform, wide rectangular flow cross section, the average water flow velocity (v_w) can be estimated from the kinematic wave celerity (c_k) using the formula (e.g. Chow *et al.* 1988):

$$v_w = \frac{3}{5}\frac{dQ}{dA} = \frac{3}{5}c_k \tag{5}$$

where Q is the river discharge and A is the flow cross-sectional area.

Model calibration and validation results

The total model simulation period extends from 2000 to 2010. However, in-situ data are only available for the period 2005 to 2010. The period with available in-situ data was split into a calibration period (2005–2007) and a validation period (2008–2010). The model was calibrated against the observed discharge at the Bahadurabad, Nuxia and Nugesha stations for the 3-year calibration period. In total, 12 parameters were automatically calibrated (6 for the upstream and 6 for the downstream portions of the basin) using a trust region reflective algorithm (Coleman & Li 1996), which outperforms the Levenberg–Marquardt algorithm if the initial parameter estimates are far from the optimum. The calibration objective function was the root mean square error (RMSE) of simulated versus observed discharge. The upstream portion of the basin was calibrated using the stations Nuxia and Nugesha, which were equally weighted in the calibration. The downstream portion of the basin was calibrated using the Bahadurabad station.

Table 2 provides an overview of the calibration parameters and the calibrated parameter values. Calibration parameters included four parameters of the Budyko rainfall–runoff model (α_1, α_2, d and S_{max}), as well as two Muskingum routing parameters (v_{max} and X). Generally, post-calibration parameter confidence intervals are reasonably confined, except

Table 1 | Overview of available virtual stations from ERS-2, Envisat and Topex over the Brahmaputra River

Target ID	Relative reading time (days)	Chainage (km)	Latitude (deg)	Longitude (deg)	SRTM (mamsl)	Delay time (days)	Delay time lower CI (days)	Delay time upper CI (days)	CC
ERS-2									
B-ERS2-1	0	304	23.049	90.436	8	62.84	44.50	66.04	0.5033
B-ERS2-2	12	220	23.669	90.360	6	9.28	5.78	11.48	0.8752
B-ERS2-3	–16	Tributary	23.954	90.928	9	5.16	2.48	7.26	0.8577
B-ERS2-4	–7	131	24.084	89.747	8	3.02	0.22	5.50	0.9234
B-ERS2-5	0	–71	25.758	89.755	20	–0.81	–2.11	1.18	0.7809
B-ERS2-6	9	–82 (tributary)	25.787	89.457	32	16.92	–10.73	18.45	0.7944
B-ERS2-7	–7	–145	26.144	90.269	36	–8.48	–22.98	–1.34	0.7917
B-ERS2-8	12	–229	26.183	90.996	38	–1.48	–3.22	–0.02	0.9219
B-ERS2-9	3	–239	26.190	91.081	41	–2.10	–4.12	0.09	0.9307
B-ERS2-10	–13	–322	26.215	91.793	44	–0.72	–3.90	1.64	0.9651
B-ERS2-11	6	–406	26.541	92.427	54	–17.95	–20.01	–4.90	0.8036
B-ERS2-12	–1	–501	26.717	93.291	72	–1.86	–4.65	–0.23	0.9637
B-ERS2-13	9	–559	26.798	93.797	78	–4.17	–5.45	–2.44	0.9390
B-ERS2-14	–17	–591	26.866	94.047	83	–4.84	–15.45	–3.79	0.9317
B-ERS2-15	–17	–599	26.973	94.075	81	–4.42	–7.30	–2.58	0.9264
B-ERS2-16	–7	–640	27.036	94.456	88	–6.84	–21.48	–3.81	0.8737
B-ERS2-17	2	–727	27.588	94.954	103	–9.08	–13.78	–5.38	0.9045
Topex									
B-Topex-1	3	60	24.686	89.687	8	–0.84	–2.67	2.04	0.9608
B-Topex-2	3	50	24.779	89.730	17	0.15	–1.99	3.51	0.9015
B-Topex-3	3	–157	26.160	90.375	34	–2.75	–4.46	0.17	0.8281
B-Topex-4	3	–161	26.193	90.391	28	–2.36	–4.91	–0.09	0.9205
B-Topex-5	5	–237	26.211	91.042	33	–2.47	–4.94	–0.23	0.9670
B-Topex-6	2	–537	26.772	93.609	76	–1.21	–3.98	1.01	0.7216
Envisat									
B-Envisat-1	0	344	22.804	90.494	0				
B-Envisat-2	0	211	23.699	90.273	6				
B-Envisat-3	–16	Tributary	23.954	90.927	5				
B-Envisat-4	0	–71	25.756	89.753	20				
B-Envisat-5	–16	–157	26.181	90.363	31				
B-Envisat-6	3	–239	26.189	91.079	37				
B-Envisat-7	6	–406	26.541	92.427	54				
B-Envisat-8	9	–559	26.798	93.798	80				
B-Envisat-9	–7	–640	27.036	94.454	86				
B-Envisat-10	12	–735	27.620	95.021	111				

for the maximum soil water storage S_{max} and the Muskingum parameter X. Figure 5 shows a comparison of simulated and observed discharge at the three stations. Model performance is generally satisfactory as evidenced by the performance statistics listed in Table 3. Root mean square errors are 42% of average discharge at Nuxia and 43% of average discharge at

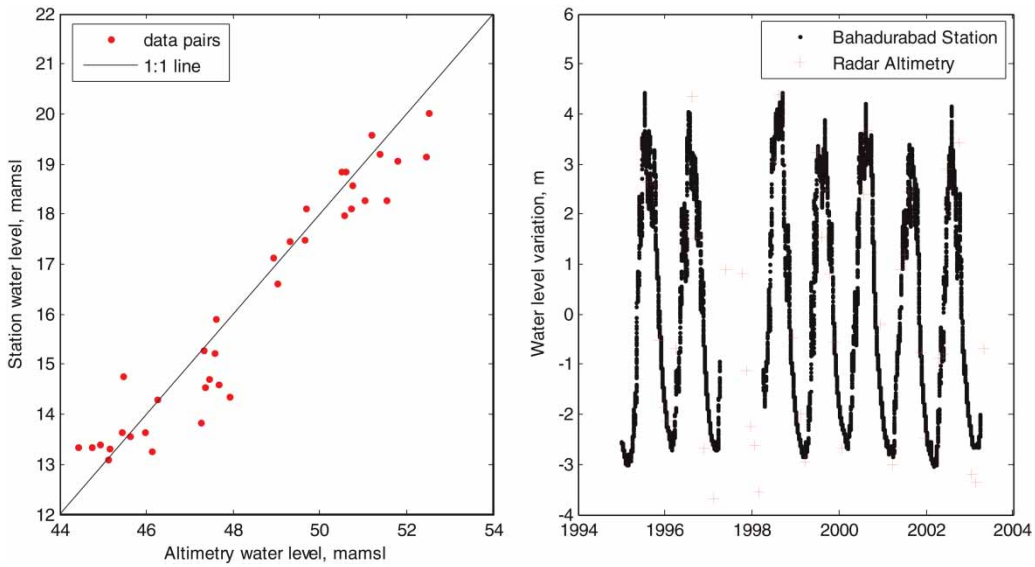

Figure 3 | Correlation between ERS-2 target 10 (B-ERS-10) and in-situ water levels at the Bahadurabad station, located 322 km downstream of the target. A time shift was applied to maximize the correlation between the two time series (see Table 1).

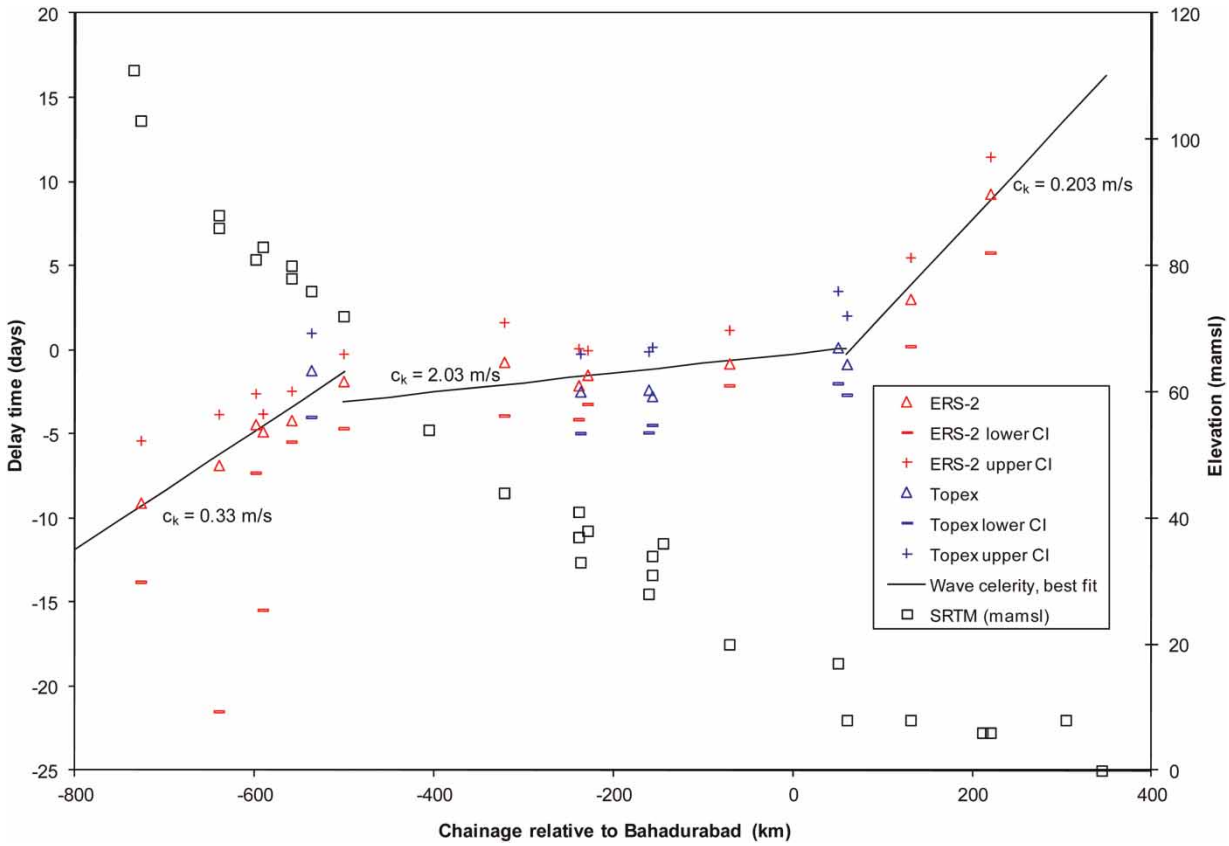

Figure 4 | Delay times between the in-situ station at Bahadurabad and all altimetry targets on the Brahmaputra River.

Table 2 | Overview of calibration parameters and calibration results

	Parameter	Description and unit	Calibrated value	Lower bound of 95% confidence interval	Upper bound of 95% confidence interval
Upstream sub-basins 1–6	α_1	Budyko parameter, governs partition between catchment retention and runoff, dimensionless	0.337	0.267	0.407
	α_2	Budyko parameter, governs partition between groundwater recharge and ET, dimensionless	0.454	0.417	0.491
	d	Baseflow recession coefficient, per day	0.0255	0.0223	0.0286
	S_{max}	Maximum soil water storage, mm	136.7	24.4	249.0
	v_w	Channel flow velocity, m per second	1.16	1.11	1.21
	X	Muskingum weighting factor, dimensionless	0.0011	–0.24	0.24
Downstream sub-basins 7–19	α_1	Budyko parameter, governs partition between catchment retention and runoff, dimensionless	0.343	0.223	0.463
	α_2	Budyko parameter, governs partition between groundwater recharge and ET, dimensionless	0.489	0.360	0.612
	d	Baseflow recession coefficient, per day	0.0138	0.0117	0.0158
	S_{max}	Maximum soil water storage, mm	145.8	44.5	247.1
	v_w	Channel flow velocity, m per second	0.86	0.789	0.907
	X	Muskingum weighting factor, dimensionless	0.0010	–0.42	0.42

Bahadurabad. Nash–Sutcliffe model efficiency ranges from 0.61 at Nugesha to 0.78 at Bahadurabad.

Data assimilation results

For the validation period (2008–2010), model performance using various gain factors G (Equation (4)) was compared to the performance of the calibrated model. The results are documented in Table 3. Without using the available altimetry data for model updating, the calibrated model achieves an NSE of 0.77 over the validation period. The model Nash–Sutcliffe efficiency can be increased to 0.83, if altimetry data are assimilated. The gain factor that yielded the highest model efficiency was $G = 0.6$. Available Envisat radar altimetry data from the time period prior to 2008 were used to establish pseudo-rating curves of simulated discharge versus altimetry levels (Figure 6). Note that the radar altimetry data from the validation period were not used in the determination of the rating curves. This was done in order to simulate operation of the model for real-time forecasting. Generally, the rating curves are consistent and the fitted parameters of the power law (Equation (3)) are reasonable. Pseudo rating curves show considerable scatter. For the validation period, the model was run in assimilation mode. The pseudo-rating curves were used to convert incoming altimetry measurements into discharge and the altimetry-derived discharge was subsequently assimilated into the model. Model performance with and without radar altimetry assimilation is shown in Figure 7. Improvements are most notable in the beginning of the base flow recession period, when the calibrated model over-estimates the discharge. This bias is effectively corrected by the data assimilation scheme.

DISCUSSION

A number of high-quality virtual stations are available on the Brahmaputra. From the ERS-2, Topex and Envisat missions, time series for 33 virtual stations were obtained over a river segment of about 1,000 km. This relatively dense spatial sampling will become even denser once data from altimetry missions, which are currently in planning or early operation stage (Cryosat-2, Sentinel-3, SWOT), become routinely available. While the temporal resolution of the available altimetry data is relatively coarse (e.g. 35 days repeat orbit for Envisat), reading times at individual targets are shifted by constant time intervals (Table 1). This implies that during the simulation period readings from at least one of the targets are available at intervals of a few days (minimum interval: 3 days, mean interval: 4.9 days, maximum interval: 13 days), which greatly augments the utility of radar

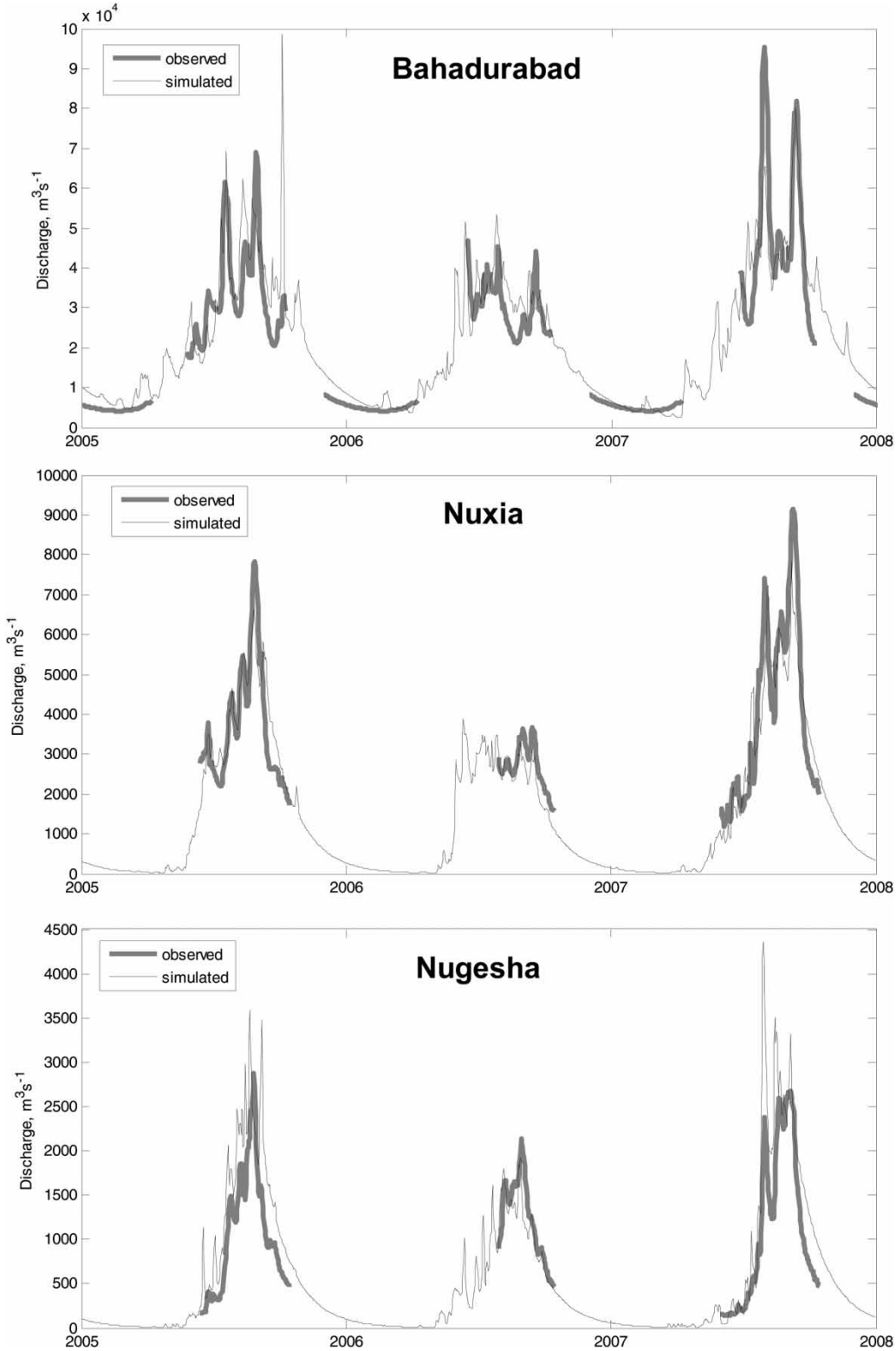

Figure 5 | Post-calibration model performance for the calibration period at the stations Bahadurabad, Nuxia and Nugesha.

Table 3 | Overview of model performance in the calibration period and in the validation period for various gain settings. Root mean square error (RMSE) and Nash–Sutcliffe model efficiency (NSE) are shown. Long-term average discharge is 20,408 $m^3 s^{-1}$ at Bahadurabad and 2,000 $m^3 s^{-1}$ at Nuxia

	RMSE, $m^3 s^{-1}$	RMSE, percent of average flow	NSE, –
Bahadurabad Calibration period	8,800	43	0.784
Nugesha Calibration period	557		0.611
Nuxia Calibration period	843	42	0.698
Bahadurabad Validation period $G = 0$	10,200	50	0.772
Bahadurabad Validation period $G = 0.1$	9,630	47	0.795
Bahadurabad Validation period $G = 0.2$	9,270	45	0.810
Bahadurabad Validation period $G = 0.3$	9,020	44	0.820
Bahadurabad Validation period $G = 0.4$	8,860	43	0.827
Bahadurabad Validation period $G = 0.5$	8,750	43	0.831
Bahadurabad Validation period $G = 0.6$	8,710	43	0.833
Bahadurabad Validation period $G = 0.7$	8,730	43	0.832
Bahadurabad Validation period $G = 0.8$	8,850	43	0.827
Bahadurabad Validation period $G = 0.9$	9,090	45	0.818
Bahadurabad Validation period $G = 1.0$	9,510	47	0.800

altimetry for flood forecasting and early warning. The near real-time altimetric monitoring capability for the Brahmaputra was significantly affected by the failure of Envisat in 2012 because this mission provided most of the operational data. The information contained in the altimetry readings can be exploited to its full potential when combined with a river basin model. The model can be used to interpolate in time and smoothen out extreme values and outliers in the altimetry dataset. The river basin model developed in this paper is relatively simple and uses a minimum amount of in-situ data. It could be improved in several ways (enhanced spatial resolution, enhanced calibration and validation, better representation of water users). Due to the coarse resolution of the model and the lack of detail in the representation of both hydrological processes and abstractions for water use, model performance is variable, when evaluated for small sub-units of the basin. However, model performance expressed in terms of RMSE and NSE is satisfactory at all three stations where in-situ data were available and is competitive compared to previous modelling efforts reported for the region (Nishat & Rahman 2009; Rao *et al.* 2009). The principal limitation for improving model performance is the quality of the precipitation forcing product. However, even at this stage the model can be successfully combined with the radar altimetry datasets to provide real-time modelling and forecasting capabilities to water resources managers. The results show that the best performance is achieved when model simulation results and radar altimetry data are weighted 40 to 60. This implies that both the model simulation and the altimetry data contain valuable information, which is combined in an optimal way in the data assimilation scheme. Data assimilation techniques are efficient tools in this context to synthesize model predictions and observations and produce the best possible estimate of model states at each point in time along with forecasts based on both model predictions and the latest available observations. The data assimilation technique used in this study is extremely simple. As a future research direction, the application of statistical data assimilation tools, such as the Ensemble Kalman Filter (EnKF), can be investigated. Possibly, model performance could be enhanced if the states of the rainfall–runoff model (i.e. root zone storage and groundwater storage) were updated in the data assimilation scheme and not only the discharges in the river network.

The presented modelling and data assimilation approach is useful as a first screening approach for large-scale river basins. The required amount of in-situ information is minimal. The model can be expanded to cover all major river

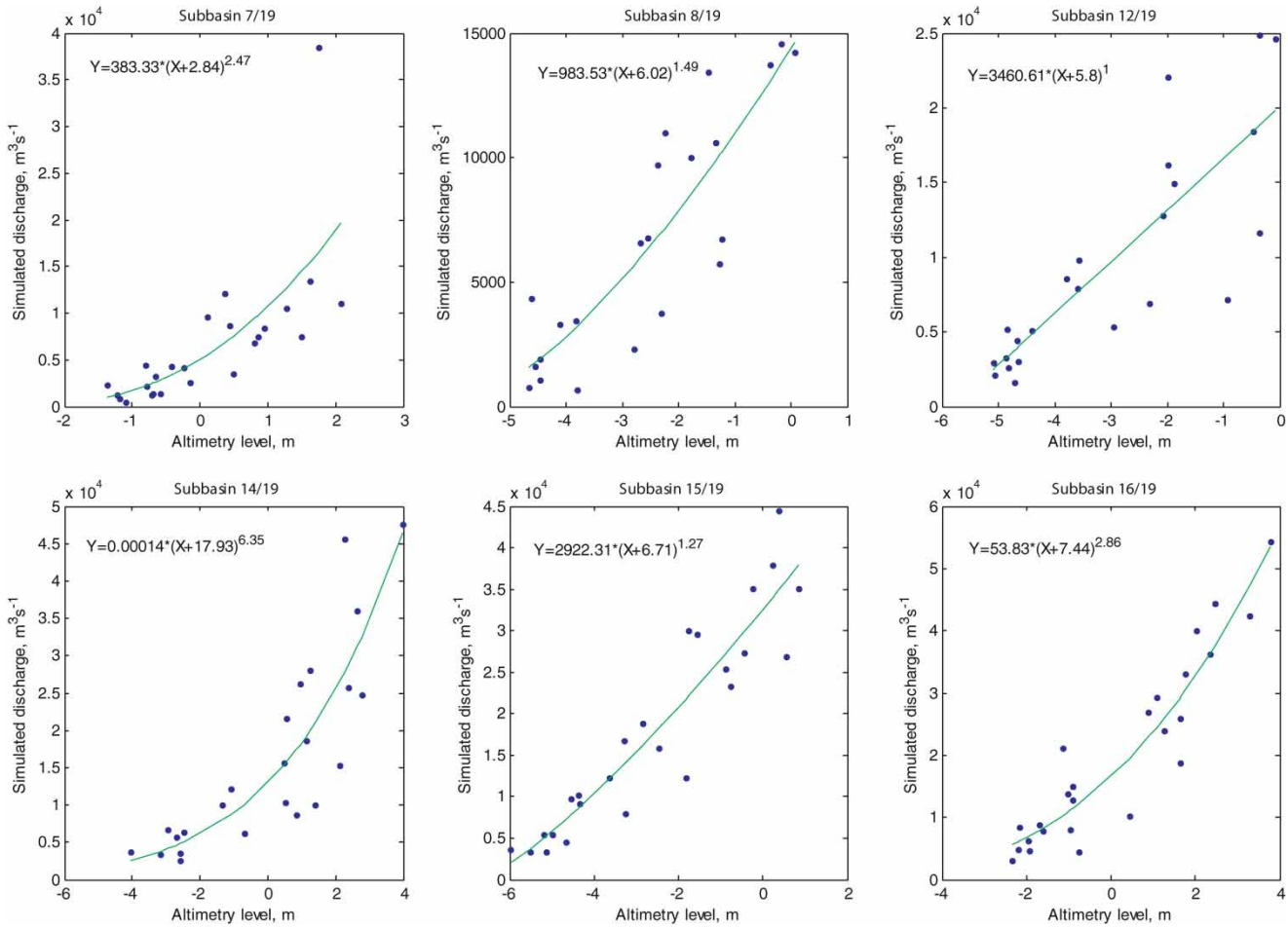

Figure 6 | Pseudo rating curves (altimetry versus simulated discharge). Only data from the calibration period are used. The fitted equations for each rating curve are shown in the plots.

basins of the world. The assimilation approach used in this study is purely heuristic. The advantages are as follows:

- Any number of altimetry targets can be efficiently assimilated into the model without increasing run-times excessively. Expensive ensemble calculations as required for the EnKF are avoided.
- The pseudo-rating curves used to convert altimetry readings into simulated discharge can be continuously updated, as more altimetry data become available.

The disadvantages are as follows:

- If the calibrated model produces biased discharge estimates that show correlated error structures, the pseudo-rating curve approach will fail. Such errors will not be mitigated by the assimilation of altimetry data. An alternative approach would be to generate rating curves based on in-situ river geometry and sparse historical discharge observations only. Such approaches have been presented in the literature and could be a promising avenue for further research (Bjerklie *et al.* 2003).
- The assimilation scheme produces discharge estimates based on both model simulation and altimetry data but does not quantify their uncertainty.

In the approach presented here, the discharge correction term (innovation) is added to only one river node, corresponding to the location of the radar altimetry target. However, due to the fact that river discharge is correlated in space, river discharge at neighbouring river nodes could be updated as well. More sophisticated data assimilation algorithms, such as the EnKF, make use of the correlation

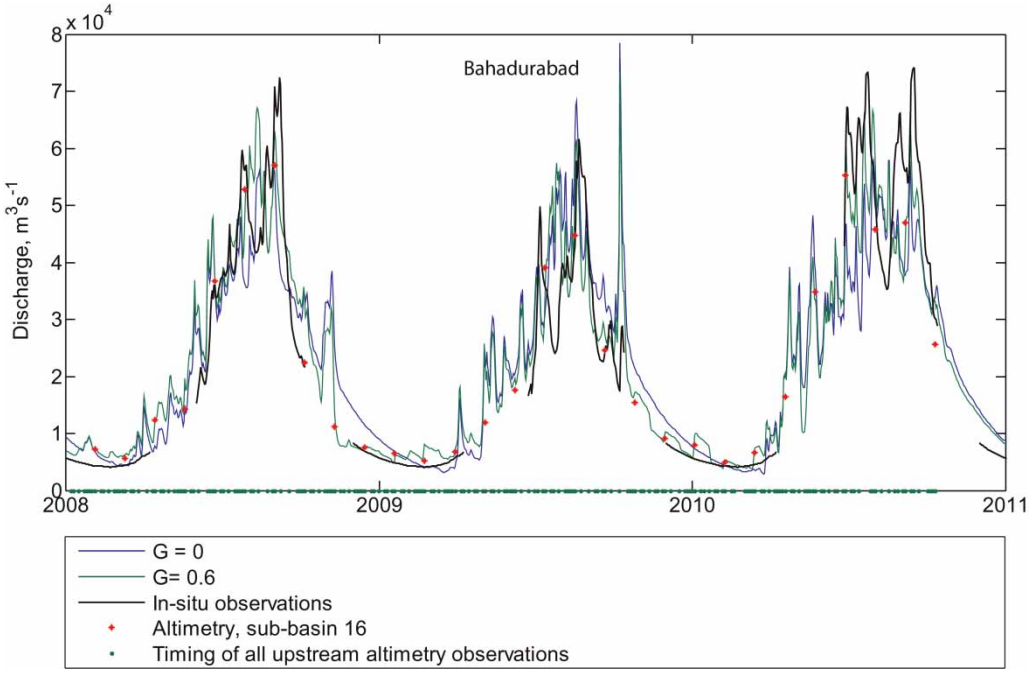

Figure 7 | Model performance at Bahadurabad with and without data assimilation for the validation period.

between a measurement and any model state. Such an approach could potentially enhance model performance significantly, particularly if internal states of the rainfall–runoff model are included in the updating scheme. An assimilation scheme based on the Kalman Filter would also provide estimates of forecast uncertainty along with the actual forecast. Such information would be extremely valuable for practical flood hazard management. However, one of the main challenges for a potential application of the Kalman Filter is the estimation of the error of the various forcing variables derived from remote sensing as well as the estimation of forcing error correlations.

CONCLUSIONS

Overall, this study has demonstrated that the combination of a river basin mass balance model and radar altimetry data leads to increased model efficiencies for predicting flood events in the Brahmaputra basin, which is an encouraging finding in view of the increase of both availability and quality of radar altimetry time series over inland waters expected over the coming years.

This work has demonstrated the availability and quality of radar altimetry water level time series over the Brahmaputra River. A river basin modelling and data assimilation approach has been developed that enables the direct use of radar altimetry data for real-time modelling and hydrological forecasting. Model efficiency increased considerably due to the assimilation of multiple radar altimetry targets.

ACKNOWLEDGEMENTS

We acknowledge the Institute of Water Modelling, Dhaka, Bangladesh, for in-situ water level data for the Bahadurabad gauging station. The authors thank the European Space Agency for supply of altimeter data.

REFERENCES

Akhtar, M. K., Corzo, G. A., van Andel, S. J. & Jonoski, A. 2009 River flow forecasting with artificial neural networks using satellite observed precipitation pre-processed with flow length and travel time information: case study of the Ganges river basin. *Hydrol. Earth Syst. Sci.* **13** (9), 1607–1618.

Alcamo, J., Doll, P., Henrichs, T., Kaspar, F., Lehner, B., Rosch, T. & Siebert, S. 2003 Development and testing of the WaterGAP 2 global model of water use and availability. *Hydrol. Sci. J.* **48** (3), 317–337.

Andreadis, K. M., Clark, E. A., Lettenmaier, D. P. & Alsdorf, D. E. 2007 Prospects for river discharge and depth estimation through assimilation of swath-altimetry into a raster-based hydrodynamics model. *Geophys. Res. Lett.* **34** (10), L10403.

Arnold, J. G., Srinivasan, R., Muttiah, R. S. & Williams, J. R. 1998 Large area hydrologic modeling and assessment – Part 1: Model development. *J. Am. Water Resour. Assoc.* **34** (1), 73–89.

Berry, P. A. M., Garlick, J. D., Freeman, J. A. & Mathers, E. L. 2005 Global inland water monitoring from multi-mission altimetry. *Geophys. Res. Lett.* **32** (16), L16401.

Biancamaria, S., Durand, M., Andreadis, K. M., Bates, P. D., Boone, A., Mognard, N. M., Rodriguez, E., Alsdorf, D. E., Lettenmaier, D. P. & Clark, E. A. 2011 Assimilation of virtual wide swath altimetry to improve Arctic river modeling. *Rem. Sens. Environ.* **115** (2), 373–381.

Birkett, C. M., Mertes, L. A. K., Dunne, T., Costa, M. H. & Jasinski, M. J. 2002 Surface water dynamics in the Amazon Basin: Application of satellite radar altimetry. *J. Geophys. Res. Atmos.* **107** (D20), 8059.

Birkinshaw, S. J., O'Donnell, G. M., Moore, P., Kilsby, C. G., Fowler, H. J. & Berry, P. A. M. 2010 Using satellite altimetry data to augment flow estimation techniques on the Mekong River. *Hydrolog. Process.* **24** (26), 3811–3825.

Bjerklie, D. M., Dingman, S. L., Vorosmarty, C. J., Bolster, C. H. & Congalton, R. G. 2003 Evaluating the potential for measuring river discharge from space. *J. Hydrol.* **278** (1–4), 17–38.

Budyko, M. I. 1958 *The Heat Balance of the Earth's Surface*. US Department of Commerce, Washington, DC.

Chow, V. T., Maidment, D. R. & Mays, L. W. 1988 *Applied Hydrology*. McGraw-Hill, Singapore.

Coe, M. T. & Birkett, C. M. 2004 Calculation of river discharge and prediction of lake height from satellite radar altimetry: Example for the Lake Chad basin. *Water Resour. Res.* **40** (10), W10205.

Coleman, T. F. & Li, Y. Y. 1996 An interior trust region approach for nonlinear minimization subject to bounds. *SIAM J. Optim.* **6** (2), 418–445.

Cretaux, J. F., Jelinski, W., Calmant, S., Kouraev, A., Vuglinski, V., Berge-Nguyen, M., Gennero, M. C., Nino, F., Del Rio, R. A., Cazenave, A. & Maisongrande, P. 2011 SOLS: A lake database to monitor in the Near Real Time water level and storage variations from remote sensing data. *Adv. Space Res.* **47** (9), 1497–1507.

Draper, A. J., Jenkins, M. W., Kirby, K. W., Lund, J. R. & Howitt, R. E. 2003 Economic-engineering optimization for California water management. *J. Water Resour. Plann. Manag. – ASCE* **129** (3), 155–164.

Dukhovny, V. A., Tuchin, A. I. & Sokolov, V. I. 2004 Decision support system for water-user associations in the Aral Sea basin. *Land and Water Management: Decision Tools and Practices* **1 and 2**, 268–274. China Agricultural Univ., Beijing.

Durand, M., Andreadis, K. M., Alsdorf, D. E., Lettenmaier, D. P., Moller, D. & Wilson, M. 2008 Estimation of bathymetric depth and slope from data assimilation of swath altimetry into a hydrodynamic model. *Geophys. Res. Lett.* **35** (20), L20401.

Global Runoff Data Center (GRDC) 2007 *Major River Basins of the World*. Koblenz, Germany.

Hargreaves, G. H. & Samani, Z. A. 1982 Estimating potential evapo-transpiration. *J. Irrigat. Drain. Div. – ASCE* **108** (3), 225–230.

Hock, R. 2003 Temperature index melt modelling in mountain areas. *J. Hydrol.* **282** (1–4), 104–115.

Hostache, R., Matgen, P., Schumann, G., Puech, C., Hoffmann, L. & Pfister, L. 2009 Water level estimation and reduction of hydraulic model calibration uncertainties using satellite SAR images of floods. *IEEE Trans. Geosci. Rem. Sens.* **47** (2), 431–441.

Huffman, G. J., Adler, R. F., Bolvin, D. T., Gu, G., Nelkin, E. J., Bowman, K. P., Hong, Y., Stocker, E. F. & Wolff, D. B. 2007 The TRMM multisatellite precipitation analysis (TMPA): Quasi-global, multiyear, combined-sensor precipitation estimates at fine scales. *J. Hydrometeorol.* **8** (1), 38–55.

Jakobsen, F., Hoque, A., Paudyal, G. N. & Bhuiyan, M. S. 2005 Evaluation of the short-term processes forcing the Monsoon river floods in Bangladesh. *Water Int.* **30** (3), 389–399.

Lagarias, J. C., Reeds, J. A., Wright, M. H. & Wright, P. E. 1998 Convergence properties of the Nelder-Mead simplex method in low dimensions. *Siam J. Optimiz.* **9** (1), 112–147.

Madsen, H. & Skotner, C. 2005 Adaptive state updating in real-time river flow forecasting – a combined filtering and error forecasting procedure. *J. Hydrol.* **308** (1–4), 302–312.

Maheu, C., Cazenave, A. & Mechoso, C. R. 2003 Water level fluctuations in the Plata basin (South America) from Topex/Poseidon Satellite Altimetry. *Geophys. Res. Lett.* **30** (3), 1143.

Mason, D. C., Bates, P. D. & Amico, J. T. D. 2009 Calibration of uncertain flood inundation models using remotely sensed water levels. *J. Hydrol.* **368** (1–4), 224–236.

Milzow, C., Krogh, P. E. & Bauer-Gottwein, P. 2011 Combining satellite radar altimetry, SAR surface soil moisture and GRACE total storage changes for hydrological model calibration in a large poorly gauged catchment. *Hydrol. Earth Syst. Sci.* **15** (6), 1729–1743.

Mondal, M. S. & Wasimi, S. A. 2006 Generating and forecasting monthly flows of the Ganges river with PAR model. *J. Hydrol.* **323** (1–4), 41–56.

Montgomery, D. R., Hallet, B., Liu, Y. P., Finnegan, N., Anders, A., Gillespie, A. & Greenberg, H. M. 2004 Evidence for Holocene megafloods down the Tsangpo River Gorge, southeastern Tibet. *Quaternary Res.* **62** (2), 201–207.

Nishat, B. & Rahman, S. M. 2009 Water resources modeling of the Ganges-Brahmaputra-Meghna River Basins using Satellite Remote Sensing Data. *J. Am. Water Resour. Assoc.* **45** (6), 1313–1327.

Nohara, D., Kitoh, A., Hosaka, M. & Oki, T. 2006 Impact of climate change on river discharge projected by multimodel ensemble. *J. Hydrometeorol.* **7** (5), 1076–1089.

Oleson, K. W., Niu, G. Y., Yang, Z. L., Lawrence, D. M., Thornton, P. E., Lawrence, P. J., Stoeckli, R., Dickinson, R. E., Bonan, G. B., Levis, S., Dai, A. & Qian, T. 2008 Improvements to the Community Land Model and their impact on the hydrological cycle. *J. Geophys. Res. – Biogeosci.* **113** (G1), G01021.

Pereira-Cardenal, S. J., Riegels, N. D., Berry, P. A. M., Smith, R. G., Yakovlev, A., Siegfried, T. U. & Bauer-Gottwein, P. 2011 Real-time remote sensing driven river basin modeling using radar altimetry. *Hydrol. Earth Syst. Sci.* **15** (1), 241–254.

Qian, T. T., Dai, A., Trenberth, K. E. & Oleson, K. W. 2006 Simulation of global land surface conditions from 1948 to 2004. Part I: Forcing data and evaluations. *J. Hydrometeorol.* **7** (5), 953–975.

Rao, K., Bhanumurthy, V. & Roy, P. S. 2009 Application of satellite-based rainfall products and SRTM DEM in hydrological modelling of Brahmaputra basin. *J. Indian Soc. Rem. Sen.* **37** (4), 587–600.

Refsgaard, J. C. & Knudsen, J. 1996 Operational validation and intercomparison of different types of hydrological models. *Water Resour. Res.* **32** (7), 2189–2202.

Rodell, M., Houser, P. R., Jambor, U., Gottschalck, J., Mitchell, K., Meng, C. J., Arsenault, K., Cosgrove, B., Radakovich, J., Bosilovich, M., Entin, J. K., Walker, J. P., Lohmann, D. & Toll, D. 2004 The global land data assimilation system. *Bull. Am. Meteorol. Soc.* **85** (3), 381–394.

Schumann, G. J. P., Neal, J. C., Mason, D. C. & Bates, P. D. 2011 The accuracy of sequential aerial photography and SAR data for observing urban flood dynamics, a case study of the UK summer 2007 floods. *Rem. Sens. Environ.* **115** (10), 2536–2546.

Schwanghart, W. & Kuhn, N. J. 2010 TopoToolbox: A set of Matlab functions for topographic analysis. *Environ. Model. Software* **25** (6), 770–781.

Stisen, S. & Sandholt, I. 2010 Evaluation of remote-sensing-based rainfall products through predictive capability in hydrological runoff modelling. *Hydrolog. Process.* **24** (7), 879–891.

Vrugt, J. A., Diks, C. G. H., Gupta, H. V., Bouten, W. & Verstraten, J. M. 2005 Improved treatment of uncertainty in hydrologic modeling: Combining the strengths of global optimization and data assimilation. *Water Resour. Res.* **41** (1), W01017.

Zhang, L., Potter, N., Hickel, K., Zhang, Y. & Shao, Q. 2008 Water balance modeling over variable time scales based on the Budyko framework – Model development and testing. *J. Hydrol.* **360** (1–4), 117–131.

First received 13 December 2011; accepted in revised form 16 March 2013. Available online 3 July 2013